

# Fast, Microwave Assisted Synthesis of Monodisperse HfO<sub>2</sub> Nanoparticles

Jonathan De Roo<sup>1,2</sup>, Katrien De Keukeleere<sup>1</sup>, Jonas Feys<sup>1</sup>, Petra Lommens<sup>1</sup>, Zeger Hens<sup>2,3</sup> and Isabel Van Driessche<sup>1</sup>

<sup>1</sup> Sol-gel Centre for Research on Inorganic Powders and Thin films Synthesis (SCRiPTS), Ghent University, Belgium

<sup>2</sup> Physics and Chemistry of Nanostructures (PCN), Ghent University, Belgium

<sup>3</sup> Center for nano and biophotonics (NB-Photonics), Ghent University, Belgium

**Address (all authors):** Krijgslaan 281 S3, 9000 Gent, Belgium

**Corresponding author:**

Isabel Van Driessche

Isabel.VanDriessche@ugent.be

Tel: 0032 9 264 44 33

Fax: 0032 9 264 49 83

**Abstract**

A conventional solvothermal synthesis was compared to a microwave assisted method for the synthesis of HfO<sub>2</sub> nanoparticles. In a microwave, the reaction could be completed in three hours, compared to three days in an autoclave. In the microwave synthesis the ensemble of particles was found to have a better size dispersion and a smaller average size (4 nm). The reaction mechanism was investigated and proof for an ether elimination process was provided. Post-synthetic modification with dopamine or dodecanoic acid permitted the suspension of the synthesized particles in both polar and apolar solvents, which is an advantage for further processing.

**keywords:** Benzyl alcohol, microwave, ligand exchange, hafnium oxide

# 1. Introduction

Hafnium oxide is a material with a number of technologically attractive properties such as a high melting point (2758 °C), a high dielectric constant ( $\approx 30$ ), a high chemical stability, a wide band gap (6 eV) and a high neutron absorption cross section. It can play a role in the continuous down-scaling of integrated circuits since new insulating materials with a high dielectric constant are being researched to replace SiO<sub>2</sub> as a gate dielectric (Wilk et al. 2001; Dahal and Chikan 2012; Molina et al. 2012a; Molina et al. 2012b; Rinkio et al. 2009). HfO<sub>2</sub> thin layers are highly promising as high- $\kappa$  dielectric layers in CMOS technology and as dielectric capacitor layers in DRAMs (Wilk et al. 2001). Hafnium oxide layers are also used as heat-resistant and highly reflective, protective optical coatings (Chow et al. 1993; Waldorf et al. 1993), as sensors (Gruger et al. 2005; Al-Kuhaili et al. 2004) and as photoluminescent materials (Elizariario et al. 2009).

In recent years, increasing research activities have been dedicated to the synthesis of metal oxide nanoparticles (Park et al. 2007; Baghbanzadeh et al. 2011). In case where large specific surface areas are required, for instance in gas sensing or catalysis, nanoparticles offer a considerable advantage over their bulk counterpart. It is also possible to tailor material properties with these nanoparticles, yielding nanocomposites. Amorphous nanoparticles of HfO<sub>2</sub> were used for EUV patterning to develop inorganic photoresists (Trikeriotis et al. 2012). Hafnia nanoparticles were embedded in a glass matrix to increase the dielectric constant (Molina et al. 2012a; Molina et al. 2012b). Recently, hafnium based nanoparticles were grown in situ in GdBa<sub>2</sub>Cu<sub>3</sub>O<sub>7.8</sub> coated conductors to improve the critical current of the superconductor (Tobita et al. 2012). Even the use in biological applications should not be excluded because of the negligible cytotoxicity of HfO<sub>2</sub> (Field et al. 2011).

Hafnium oxide nanoparticles have already been synthesized with a variety of methods, such as surfactant based (Dahal and Chikan 2012; Tang et al. 2004; Chaubey et al. 2012; Tirosh and Markovich 2007), hydrothermal (Stefanic et al. 2005), microwave assisted hydrothermal (Elizariario et al. 2009), ultrasonically assisted hydrothermal (Meskin et al. 2007), solvothermal (Pinna et al. 2004; Pucci et al. 2009; Boyle et al. 2012; Buha et al. 2010), precipitation (Ramadoss et al. 2012) and sonochemical synthesis (Ramadoss and Kim 2012). However, most of these methods are unfavorable because of a long reaction time, a broad size distribution, the agglomerated state of the particles or the large diameter. In addition, there is often need for a second calcination step to crystallize the particles which aggravates agglomeration (Chaubey et al. 2012; Boyle et al. 2012; Ramadoss et al. 2012). Some synthesis methods (Dahal and Chikan 2012; Tang et al. 2004) yield unagglomerated and crystalline (sub 10 nm) particles but have the drawback that they use large quantities of surfactants and expensive precursors. Hence, the particles are coated with these surfactants and are therefore only soluble in apolar solvents.

In this work, we envisage applications that require a monodisperse ensemble of sub 10 nm particles in a inorganic matrix. This is the case for the inclusion in, e.g., thermo-electric materials (Huang et al. 2004) or High Temperature Superconductors (HTS) (Obradors et al. 2012; Matsumoto and Mele 2010). Due to the high chemical stability and the high melting point, hafnia is an ideal candidate for these kind of composites. In order to incorporate the nanoparticles, they need to be colloiddally stable in the precursor solution of the inorganic matrix. In case of High Temperature Superconductors these solutions are mostly water (Van Driessche et al. 2012) or methanol (Obradors et al. 2012) based.

An interesting solvothermal synthesis was presented by Buha *et al.* They were able to form HfO<sub>2</sub> particles at a low temperature (220 °C) starting from the relatively economical material HfCl<sub>4</sub> (Buha et al. 2010). The synthesis uses benzyl alcohol as a solvent, which is an environmentally friendly chemical that is used in the food industry. However the synthesis of Buha *et al.* has some serious drawbacks such as a long reaction time, a broad size distribution

and an agglomerated state of the particles. In this paper we present a method to overcome these limitations. To speed up the reaction and to obtain smaller size dispersions, we use a microwave assisted solvothermal synthesis. Microwaves couple directly to the molecules in the reaction mixture, resulting in a more efficient energy transfer and an often significant enhancement of the reaction rate (Kappe and Stadler 2005; Gabriel et al. 1998; Dahal et al. 2012). Metal oxide nanoparticle synthesis in a microwave is already reported (Baghbanzadeh et al. 2011; Bilecka et al. 2011; Bilecka et al. 2008) but to the best of our knowledge no literature is available for HfO<sub>2</sub> nanoparticles. We also investigated the reaction mechanism in both the autoclave and the microwave reaction. In contrast to the suggestion of Buha *et al.* we found proof of an ether elimination reaction in the autoclave synthesis. In the microwave synthesis, several side products were identified but the principal reaction mechanism remains the ether elimination. To tackle agglomeration problems and to allow dispersion of the particles in various types of solvents, the surface of the particles was coated with either dopamine or dodecanoic acid. The post-synthetic modification of benzyl alcohol synthesized particles was already reported for iron oxide, zirconia and indium tin oxide (Grote et al. 2012; Pinna et al. 2005). For the first time, related approaches are reported here for hafnium oxide nanoparticles. Despite the similarities between zirconium and hafnium, we observed some profound differences.

## 2. Experimental

### 2.1. Synthesis procedures

HfCl<sub>4</sub> (99.9 % - Alfa Aesar), anhydrous benzyl alcohol (99.8 % - Sigma-Aldrich), triethanolamine (98+ % - Alfa Aesar), oleylamine (80-90 % C18, 97 % primary amine - Acros), dodecanoic acid (99 % - Sigma-Aldrich) were used without further purification. Hafnium chloride was stored in a desiccator for short term use and in a glove box with less than 1 ppm water for long term storage.

To synthesize HfO<sub>2</sub> particles in an autoclave, the solvothermal synthesis developed by Niederberger and applied by Buha *et al.* was adopted (Buha et al. 2010). Typically 0.2 g of HfCl<sub>4</sub> was added to 45 mL of benzyl alcohol in a stainless steel autoclave with Teflon liner. The autoclave was sealed with screws and heated in an oven to 220 °C for 3 days. The resulting precipitate was washed with ethanol and diethylether.

In a typical microwave synthesis 4.5 mL of benzyl alcohol was added to HfCl<sub>4</sub> so that the final concentration was about 0.03 M. The mixture was stirred at room temperature to disperse the HfCl<sub>4</sub> powder in benzyl alcohol. For further dissolution, the mixture was heated in the microwave to 60 °C for 5 minutes. Finally, the solution was quickly heated to 220 °C. The microwave device was of the type CEM discover equipped with an auto sampler and IR temperature detection. A typical temperature/power/pressure profile is provided in the supporting information (SI). After reaction, diethyl ether was added and the particles were retrieved via centrifugation and dispersed in ethanol.

Post-modification with dodecanoic acid was found to yield the best result with an initial HfCl<sub>4</sub> concentration of 0.09 M. First, the particles were precipitated with diethyl ether and redispersed in chloroform. 40 mg of dodecanoic acid was added and stirred for 5 min. The addition of 50 µL of oleylamine yields a clear and colorless suspension. The particles were precipitated with a non-solvent and dispersed in apolar solvents.

Post-modification with dopamine was executed by adding 15 mg to the reaction mixture after microwave synthesis and stirring at 60 °C. The precipitates could be redispersed in water. They were purified by adding tetramethylammonium hydroxide, centrifugation and subsequent suspension in slightly acidic distilled water.

## 2.2. Analysis techniques

For Dynamic Light Scattering (DLS) and zeta potential measurements a Malvern Nano ZS was used in backscattering mode (173°). Quantitative analysis of metals was obtained by calibration of a Rigaku CG EDXRF analyzer working with the FP quantitative analysis (RPF-SQX). TEM measurements were performed on a JEOL JEM-2200FS TEM with Cs corrector. NMR spectra were recorded with a Bruker 500 MHz AVANCE III spectrometer equipped with a BBI-probe. Qualitative GC-MS experiments were performed on a Hewlett Packard G1800B GCD and quantitative measurements for organic compounds were obtained from a Hewlett Packard 5890 CD2 GC with FID detection. Statistical analysis was performed with SPSS Statistics 19. For XRD characterization a Thermo Scientific ARL X'tra X-ray diffractometer was used with the CuK $\alpha$  line as the primary source. To estimate the crystallite diameter from the XRD diffractogram, the Scherrer equation was applied

$$d = \frac{0.95 \lambda}{B \cos \theta}$$

where  $\lambda$  is the wavelength of the X-rays,  $\theta$  is the diffraction angle and  $B$  is related to the width  $\Delta$  of the Gaussian fit by

$$B = \frac{4\pi}{360} \Delta \sqrt{\ln 2}$$

## 3. Results

### 3.1. Autoclave synthesis

To properly compare the microwave synthesis developed here with a conventional heating approach, first the solvothermal synthesis of Buha *et al.* was executed and fully characterized. After three days at 220 °C, a precipitate was retrieved from the autoclave, washed and suspended in ethanol. From the TEM image in Fig. 1a it can be noted that the suspension consists of ellipsoidal nanoparticles with an varying aspect ratio between 0.5 and 0.9. Since the particles have no uniform shape, we use the *effective diameter* to analyze sizes and asses size distributions. This effective diameter is determined as the diameter of a 2D circle with the same surface area as the projection of the particle obtained in the TEM image. A statistical representation of the size distribution was made based on a significantly large population of particles (Fig. 1b). This distribution matched well with the applied Gaussian fit. The average effective diameter is 5.2 nm with a standard deviation of 1.5 nm, giving a size dispersion of  $\pm 30$  %. However, it is already indicated by the TEM images that the particles form large aggregates. This confirmed by DLS measurements on the suspensions (SI). Agglomeration is very unfavorable for applications where a uniform distribution of individual particles in a matrix is required.

**Fig. 1** Characterization of the HfO $_2$  particles, solvothermally prepared in the autoclave. (a) TEM image (b) size distribution obtained from TEM (c) powder XRD diffractogram

The crystallinity of the nanoparticles is confirmed by the XRD diffraction pattern, in which the monoclinic phase is recognized and the different planes were indexed, see Fig. 1c. Due to the small size of the particles, the reflections in the XRD pattern are broadened and often overlap. Nevertheless, the (-111) and the (111) reflections remain fairly isolated and their width can be

associated with the diameter  $d_{XRD}$  of the crystallites by the Scherrer equation. For the (-111) reflection we find  $d_{XRD} = 6.3 \text{ nm}$  and for the (111) reflection  $d_{XRD} = 8 \text{ nm}$ . Although the method clearly overestimates the absolute size in this case (vide supra), it again points out the anisotropy of the particles. The observed differences of  $d_{XRD}$  for the (-111) and (111) planes indicate that there is a larger periodicity of the (111) planes, compared to the (-111) planes. Indeed, this is confirmed by HRTEM measurements (Fig. 2). From the Fourier transform of the image and measurements in real space, the interplanar distance was determined and related to the appropriate XRD reflection. One can now clearly see that the (-111) planes are directed parallel to the long axis of the ellipsoid and the (111) planes parallel to the short axis. Hence, the periodicity of the (111) planes is more extensive, resulting in a more narrow XRD reflection.

**Fig. 2** HRTEM images of the HfO<sub>2</sub> particles, solvothermally prepared in an autoclave. The inset shows the Fourier Transform (FFT) of the image.

After synthesis, stability measurements on the suspensions in ethanol were performed and a positive zeta potential (+47 mV) was observed. Notwithstanding this very high value, a considerable fraction of the nanoparticles precipitates and it was only possible to stabilize the particles in extremely diluted conditions. Even then, the particles themselves are not stabilized but rather form large agglomerates, as seen in DLS measurements (SI).

### 3.2. Microwave synthesis

The same conditions as in the autoclave synthesis (temperature and filling ratio) were applied in the microwave assisted synthesis. The reaction time was systematically increased from 1 to 3 hours and of each sample the reaction yield and the effective diameter were estimated via XRF and TEM, respectively. The results are displayed in Fig. 3 and it is clear that almost full yield is obtained after three hours. This is a significant reduction in reaction time compared to the autoclave synthesis (3 days). After two hours the average effective diameter changes only slightly but the yield goes up from about 75 % to almost 100 %.

**Fig. 3** Yield and size evolution in function of the reaction time in a microwave assisted set up

The microwave prepared particles have an ellipsoidal shape, as is confirmed by TEM images (Fig. 4a). So at this point, there is no difference with the autoclave synthesized particles. However, the average effective diameter of the microwave prepared particles (Fig. 4b) is smaller and the size distribution is much more narrow. The average diameter of the microwave particles is 4 nm compared to 5.2 nm for the autoclave particles. The standard deviation of the Gaussian fit is also reduced from 1.5 to 0.86 nm, giving a size dispersion of  $\approx 20\%$ . So we can conclude that the microwave synthesis yields smaller and more monodisperse hafnium oxide nanoparticles than the autoclave synthesis. In addition, the reaction time is considerably shorter. Prolonged reaction times (up to 12 hours) in the microwave do not yield significant changes in shape or size distribution of the particles, which indicates that the observed differences with the autoclave synthesis are not caused by different reaction times.

**Fig. 4** Characterization of the HfO<sub>2</sub> particles, obtained after 3 hours of microwave assisted solvothermal synthesis. (a) TEM image (b) size distribution (c) powder XRD pattern of particles obtained after 1, 2 and 3 hours of reaction

In Fig. 4c, XRD diffractograms of the particles at different stages of the reaction are displayed. Although the particles show already some crystallinity after two hours, the quality of the XRD diffractogram considerably improves during the last hour of reaction. Again, the peaks are broadened extensively and show often overlap, even more than in Fig. 1c. This can be explained by the smaller average size and the smaller size distribution. The latter is important since larger particles contribute more to a sharp and clear peak. In an autoclave synthesis, the maximum effective diameter is about 8 nm while for the microwave synthesis this is 5 nm. The high crystallinity of the particles is confirmed by the high resolution TEM images where well developed lattice fringes are visible (Fig. 5). Again, it was found that the (111) planes are parallel to the short axis of the ellipsoidal particle, so the growth direction was not changed by applying microwave heating.

**Fig. 5** HRTEM images of the HfO<sub>2</sub> particles, solvothermally prepared in the microwave. The inset shows the FFT of the image

Regarding the stability of the suspension of microwave prepared particles in ethanol, an average zeta potential of + 25 mV was measured. This is lower compared to the zeta potential of the autoclave synthesized particles (+ 47 mV). Hence, the microwave prepared particles form less stable suspensions. Additional zeta potential measurements in water were performed to estimate the iso-electric point of hafnium oxide, which to our knowledge has never been determined. To keep the ionic strength constant for all measurements, all samples contain 0.01 M NaCl and the pH was adjusted via 0.01 M HCl and 0.01 M NaOH solutions. The average zeta potential and the standard deviation at different pH values are depicted in Fig. 6. The data are closely described by a sigmoidal function, which goes through zero at pH = 8.3, thereby identifying the iso-electric point. To ensure good colloidal stability, the absolute value of the zeta-potential needs to be higher than 25 mV. Therefore, we conclude from the graph that stable suspensions of hafniumoxide nanoparticles are feasible at pH values lower than 6 or higher than 10.

**Fig. 6** Determination of the iso-electric point of hafnium oxide, Zeta potential measurements at different pH values

### 3.3. Stability improvement of colloidal suspensions

Although all samples which have a zeta potential of more than 25 mV should in principle be colloidally stable, large agglomerates of particles are present in suspension as indicated by DLS (SI). To obtain a suspension of individual particles, several strategies were applied. The addition of triethanolamine before microwave treatment resulted in amorphous but well dispersed hafnia particles (SI). Regarding their applications, crystallinity is however indispensable for the particles. They need to be perfectly stable and inert in, e.g., a REBa<sub>2</sub>Cu<sub>3</sub>O<sub>7- $\delta$</sub>  (RE = rare earth) precursor solution since the harsh growth conditions of the superconductor could otherwise lead to agglomeration or dissolution of the particles. Therefore, another procedure was selected. The synthesis itself was not altered but after synthesis the surface of the already crystalline particles was modified to break up the clusters in non-agglomerated particles. The advantage of post-synthetic modification over a direct surfactant assisted synthesis is that much less surfactant is needed. Dopamine has already been shown to stabilize titania and iron oxide in situ (Pinna et al. 2005; Niederberger et al. 2004a) and to provide solubility in polar solvents. Long chain carboxylic acids on the other hand were used by researchers to solubilize indium-tin oxide and zirconia nanoparticles in apolar solvents after a benzyl alcohol solvothermal synthesis (Grote et al. 2012).

We modified the surface of the synthesized particles both with dopamine and dodecanoic acid. In contrast to the case of  $\text{ZrO}_2$  described by Grote *et al.* the addition of dodecanoic acid did not bring the particles fully in suspension. It was found necessary to add a little amount of oleylamine to the solution. By following this procedure, the surface modification lasts only five minutes and yields a completely transparent solution in chloroform. It was decided to use chloroform as a solvent instead of hexane or toluene because of the high solubility of benzyl alcohol in chloroform. Hence, the desorption of benzyl alcohol during the post-synthetic modification is favored. Note that in order to obtain a completely transparent dispersion, the concentration of  $\text{HfCl}_4$  in the initial reaction mixture is critical: 0.09 M versus 0.03 M is equal to transparent versus turbid.

Post-synthetic modification with dopamine was performed in a different fashion than the procedure of Pinna *et al.* If the  $\text{HfO}_2$  particles were precipitated after synthesis, it was not possible to bring them in suspension with dopamine. Dopamine was therefore added to the reaction mixture, directly after microwave synthesis and the resulting precipitate could be redispersed in water. TEM images of particles functionalized with either dodecanoic acid or dopamine are provided in Fig. 7. From these figures, it is seen that the dodecanoic acid functionalized particles are clearly separated on the TEM grid due to steric stabilization by the ligand. Although there is a significant improvement compared to Fig. 4a, this is less clear for the dopamine functionalized particles.

**Fig. 7** Characterization of the  $\text{HfO}_2$  particles, obtained after post-modification with (a) dodecanoic acid and oleylamine and (b) dopamine

To confirm the success of the post-synthetic modification, DLS measurements were performed. In Fig. 8 clusters of 60 nm are visible in an unfunctionalized sample (solvent = ethanol). This is in contrast to the distribution of dopamine functionalized particles which is centered around 10 nm. This advocates a successful post-synthetic modification. It is noted that the size is slightly overestimated. However, DLS provides a hydrodynamic diameter, not the real size. In addition, the model assumes spherical particles which is here clearly not the case. The particles functionalized with dodecanoic acid were also observed to be smaller than the clusters of as-synthesized particles (Fig. 8). However it was already clear from TEM images that the dodecanoic acid functionalized particles are clearly separated.

**Fig. 8** DLS measurement of unfunctionalized particles in ethanol, particles functionalized with dodecanoic acid and dispersed in chloroform and dopamine functionalized particles in water

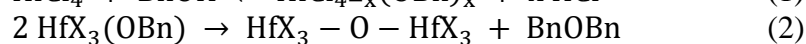
After successfully obtaining the suspension of colloiddally stable hafnium oxide nanoparticles, these particles are now ready for applications where monodisperse batches of crystalline, nanoscale hafnia particles are required. For instance, the dopamine functionalized particles are stable in water and can therefore be used for incorporation in High Temperature Superconductors via water-based approaches (Feys *et al.* 2012).

## 4. Discussion

It is clear from the results that there are some profound differences between a solvothermal and a microwave assisted synthesis technique whereas other features are not altered by the change

of heating system. In both cases, crystalline particles in the monoclinic phase were retrieved. From high resolution TEM measurements we derived that also the orientation of the crystallographic planes inside the ellipsoidal particles is identical in both synthesis methods. The (-111) planes are parallel to the long axis of the ellipsoid and the (111) planes parallel to the short axis. In contrast to these similarities, the reaction time in the microwave setup is much shorter (3 hours versus 3 days). The microwave synthesized particles are also smaller and have a smaller size dispersion.

To investigate whether these differences reflect a change in reaction mechanism, we analyzed the reaction mixture of both the autoclave and the microwave assisted synthesis. Concerning the HfO<sub>2</sub> synthesis in an autoclave, Buha *et al.* suggested a reaction mechanism based on a benzyl chloride elimination (Buha *et al.* 2010). However, the only species that we could identify in the autoclave reaction mixture, both by GC-MS and NMR analysis (SI), were benzyl alcohol and dibenzyl ether. Especially the presence of dibenzyl ether suggests a different two-step process. We propose that in the first step, a ligand exchange takes place according to Eq. 1, where the chloride is (partly) replaced by benzyl alcoholate. In the second step, the oxygen is provided to the metal via an ether elimination reaction (Eq. 2). In this equation, the ligands not participating in the reaction are represented by "X". This mechanism is very similar to what was proposed for the synthesis of oxide nanoparticles with alkoxides as a reagent (Pinna *et al.* 2004; Olliges-Stadler *et al.* 2010). The observed quantity of ether (80 % of the reaction mixture) is however much larger than expected if only the oxide formation reaction would have proceeded. This has also been observed for a comparable SnO<sub>2</sub> synthesis and it was assumed that the synthesized metal oxide could catalyze the etherification (Niederberger and Garnweitner 2006). However, a more straightforward explanation for the extensive ether formation is the acid catalyzed condensation of alcohols (Eq. 3). This reaction typically requires a strong acid and elevated temperatures. In our case, the acid (HCl) is provided by the ligand exchange reaction (Eq. 1).



GC and NMR measurements were also conducted on the microwave reaction mixture. In <sup>13</sup>C NMR, only benzyl alcohol and dibenzyl ether were detected (SI). In <sup>1</sup>H NMR some additional low intensity resonances were observed but their interpretation was not straightforward (SI). Some authors lower the concentration of BnOH to get a better NMR signal of the other compounds (Niederberger *et al.* 2004b). We however refrain from doing so since it might alter the reaction mechanism. GC-MS has a lower detection limit and could identify various new compounds that were not detected in the autoclave reaction mixture. In table 1 the different reaction products and their molar percentage (as determined from GC-FID) are displayed. The analysis was repeated several times so we could calculate a mean and a standard deviation. We also performed and analyzed a reaction of 0.12 M HCl in BnOH at 220 °C in the microwave, where the amount of HCl used, is equivalent to a full ligand exchange of 0.03 M HfCl<sub>4</sub> to Hf(OBn)<sub>4</sub>.

**Table 1** The molar percentages of different products identified in the microwave reaction mixture by gas chromatography. Two types of experiments were studied. Sample **1** with 0.03 M HfCl<sub>4</sub> in 4.5 mL BnOH and sample **2** with an equivalent amount of HCl (0.12 M). The analyses were repeated several times and a mean and a standard deviation were calculated

1 0.03 M HfCl <sub>4</sub>	2 0.12 M HCl
----------------------------	--------------



BnCl	0.19 ± 0.10	0.17 ± 0.04
BnOH	69.2 ± 1.50	63.4 ± 0.40
BnOBn	29.2 ± 1.50	34.9 ± 0.50
$\phi - CH = CH - \phi$	0.42 ± 0.02	0.37 ± 0.00
$\phi - CH_2 - \phi - CH_2 - OH$ ( <i>p</i> )	0.15 ± 0.02	0.14 ± 0.01
$\phi - CH_2 - \phi - CH_2 - OH$ ( <i>m</i> )	0.15 ± 0.01	0.18 ± 0.01
$\phi - CH_2 - \phi - CH_2 - OH$ ( <i>p</i> )	0.51 ± 0.04	0.60 ± 0.00
$\phi - CH_2 - CH_2 - \phi$	0.16 ± 0.03	0.19 ± 0.00

From the table, it is clear that the main reaction product is dibenzyl ether, next to unreacted benzyl alcohol. As commented earlier, this is mostly likely due to the reaction in Eq. 3. Dibenzyl ether could also be the result of Eq. 2. It is noted that much less dibenzyl ether is present in the microwave reaction mixture (30 %) compared to the autoclave reaction mixture (80 %). The explanation probably lies in the shorter reaction time of the microwave synthesis.

Apart from the compounds already found in the autoclave, in the microwave HfO<sub>2</sub> reaction mixture (sample **1**) other molecules such as benzyl chloride are present that could be elimination products of an oxide formation (Eq. 4). However, benzyl chloride is also observed in the sample with pure HCl (sample **2**), see table 1. BnCl can be formed via Eq. 5, an S<sub>N</sub>1 reaction of BnOH with HCl. Indeed, The 'OH' leaving group is activated by a proton and subsequently detached from the molecule. The intermediate benzylic cation is sufficiently stabilized by delocalization over the aromatic ring. Attack of the nucleophilic chloride on the cation results then in the formation of BnCl. So BnCl could be formed during oxide formation but it could also be formed by HCl which is released in the ligand exchange. This complicates the analysis. In addition, the same reasoning can be applied for all the other compounds listed in Table 1. All are present in the sample **2**.

To identify significant differences, an independent-samples T Test was performed. On the 95 % confidence level, it was concluded that the amounts of BnOH, BnOBn and stilbene ( $\phi - CH = CH - \phi$ ) are significantly different in sample **1** and **2**. The lower concentration of BnOBn in sample **1**, is probably the result of a slow ligand exchange while in sample **2** the full amount of HCl is already provided from the beginning of the reaction. The higher concentration of stilbene in sample **1** could mean that it is involved in the oxide formation. In literature, the formation of 1-ethoxy-1,2-diphenylethane ( $\phi - CH - CH(OH) - \phi$ ) was observed in the synthesis of Nb<sub>2</sub>O<sub>5</sub> and explained by the transition state (TTS) in Fig. 9 (Niederberger and Garnweitner 2006). We can assume that the TTS applies also in our case but in contrast to the synthesis of Nb<sub>2</sub>O<sub>5</sub>, we work in acidic medium. Hence the formed 1-ethoxy-1,2-diphenylethane undergoes a subsequent elimination reaction to cis-stilbene ( $\phi - CH = CH - \phi$ ), see Eq. 6. The mechanism for this reaction is explained in detail in the supporting information.

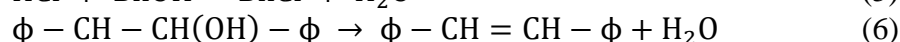
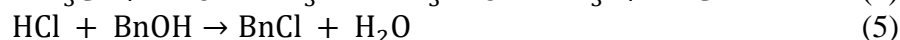
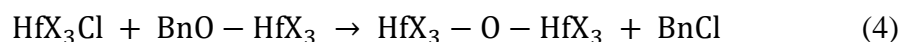


**Fig. 9** The transition state to explain the formation of  $\phi - CH - CH(OH) - \phi$

Although the absolute amount of stilbene is too low to ascribe the oxide formation fully to that mechanism, it will probably play a role. However, the most important reason for the observed differences between autoclave and microwave synthesis will most likely be purely kinetic. In a microwave reaction, the final reaction temperature of 220 °C is reached at a heating rate of 40

°C/min. The oven in which the autoclave is placed has a slow heating rate of 4.5 °C/min. Even when the furnace reaches the final temperature, the reaction mixture itself is not yet equilibrated. Microwaves are much more efficient since they couple directly to the molecules. This considerable difference in heating rate could have an influence on the nucleation and growth process, thereby leading to smaller and monodisperse particles in the microwave. In addition, we believe that the presence of the new compounds in the microwave reaction mixture (Table 1) could be caused by local superheating effects. This enables reactions to overcome activation energies which are too high in situations of thermal equilibrium.

## 5. Conclusion

In this paper we report on the comparison of a microwave assisted solvothermal synthesis of HfO<sub>2</sub> nanoparticles with a conventional heating system (autoclave). The results of the solvothermal synthesis of Buha *et al.* proved to be reproducible but we found evidence for another reaction mechanism, involving an ether elimination. Compared to an autoclave synthesis, the microwave synthesis is much faster and yields more monodisperse, smaller particles. The reaction mechanism was again investigated but the use of chlorides as reagents make the analysis very difficult. By ligand exchange with benzyl alcohol, HCl is formed and can catalyze reactions that yield the same compounds as the oxide formation reaction. In order to obtain non-agglomerated particles, post-synthetic modification was successfully performed with a dodecanoic acid or dopamine. In that way it was possible to disperse the hafnia nanoparticles either in apolar or polar solvents for further processing.

## 6. Acknowledgements

Prof. J. C. Martins and Freya Van den Broeck are acknowledged for NMR measurements. Jan Goeman is greatly thanked for GC analysis. We are grateful to Prof. De Smedt for use of the zetasizer and Bart Lukas for training. Stijn Flamee and Glenn Pollefeyt are acknowledged for TEM training.

## References

- Al-Kuhaili MF, Durrani SMA, Khawaja EE (2004) Characterization of hafnium oxide thin films prepared by electron beam evaporation. *J Phys D-Appl Phys* 37 (8):1254-1261. doi:10.1088/0022-3727/37/8/015
- Baghbanzadeh M, Carbone L, Cozzoli PD, Kappe CO (2011) Microwave-Assisted Synthesis of Colloidal Inorganic Nanocrystals. *Angewandte Chemie International Edition* 50 (48):11312-11359. doi:10.1002/anie.201101274
- Bilecka I, Djerdj I, Niederberger M (2008) One-minute synthesis of crystalline binary and ternary metal oxide nanoparticles. *Chem Commun* (7):886-888. doi:10.1039/b717334b
- Bilecka I, Luo L, Djerdj I, Rossell MD, Jagodic M, Jaglicic Z, Masubuchi Y, Kikkawa S, Niederberger M (2011) Microwave-Assisted Nonaqueous Sol-Gel Chemistry for Highly Concentrated ZnO-Based Magnetic Semiconductor Nanocrystals. *Journal of Physical Chemistry C* 115 (5):1484-1495. doi:10.1021/jp108050w

- Boyle TJ, Steele LAM, Burton PD, Hoppe SM, Lockhart C, Rodriguez MA (2012) Synthesis and Structural Characterization of a Family of Modified Hafnium tert-Butoxide for Use as Precursors to Hafnia Nanoparticles. *Inorg Chem* 51 (22):12075-12092. doi:10.1021/ic300622h
- Buha J, Arcon D, Niederberger M, Djerdj I (2010) Solvothermal and surfactant-free synthesis of crystalline Nb<sub>2</sub>O<sub>5</sub>, Ta<sub>2</sub>O<sub>5</sub>, HfO<sub>2</sub>, and Co-doped HfO<sub>2</sub> nanoparticles. *Phys Chem Chem Phys* 12 (47):15537-15543. doi:10.1039/c0cp01298j
- Chaubey GS, Yao Y, Makongo JPA, Sahoo P, Misra D, Poudeu PFP, Wiley JB (2012) Microstructural and thermal investigations of HfO<sub>2</sub> nanoparticles. *RSC Adv* 2 (24):9207-9213. doi:10.1039/c2ra21003g
- Chow R, Falabella S, Loomis GE, Rainer F, Stolz CJ, Kozlowski MR (1993) Reactive evaporation of low-defect density hafnia. *Appl Optics* 32 (28):5567-5574
- Dahal N, Chikan V (2012) Synthesis of Hafnium Oxide-Gold Core-Shell Nanoparticles. *Inorg Chem* 51 (1):518-522. doi:10.1021/ic201977d
- Dahal N, Garcia S, Zhou JP, Humphrey SM (2012) Beneficial Effects of Microwave-Assisted Heating versus Conventional Heating in Noble Metal Nanoparticle Synthesis. *ACS Nano* 6 (11):9433-9446. doi:10.1021/nn3038918
- Elizariario SA, Cavalcante LS, Sczancoski JC, Pizani PS, Varela JA, Espinosa JWM, Longo E (2009) Morphology and Photoluminescence of HfO<sub>2</sub> Obtained by Microwave-Hydrothermal. *Nanoscale Res Lett* 4 (11):1371-1379. doi:10.1007/s11671-009-9407-6
- Feys J, Vermeir P, Lommens P, Hopkins SC, Granados X, Glowacki BA, Baecker M, Reich E, Ricard S, Holzappel B, Van der Voort P, Van Driessche I (2012) Ink-jet printing of YBa<sub>2</sub>Cu<sub>3</sub>O<sub>7</sub> superconducting coatings and patterns from aqueous solutions. *J Mater Chem* 22 (9):3717-3726. doi:10.1039/c1jm14899k
- Field JA, Luna-Velasco A, Boitano SA, Shadman F, Ratner BD, Barnes C, Sierra-Alvarez R (2011) Cytotoxicity and physicochemical properties of hafnium oxide nanoparticles. *Chemosphere* 84 (10):1401-1407. doi:10.1016/j.chemosphere.2011.04.067
- Gabriel C, Gabriel S, Grant EH, Halstead BSJ, Mingos DMP (1998) Dielectric parameters relevant to microwave dielectric heating. *Chem Soc Rev* 27 (3):213-223. doi:10.1039/a827213z
- Grote C, Cheema TA, Garnweitner G (2012) Comparative Study of Ligand Binding during the Postsynthetic Stabilization of Metal Oxide Nanoparticles. *Langmuir* 28 (40):14395-14404. doi:10.1021/la301822r
- Gruger H, Kunath C, Kurth E, Sorge S, Pufe W Study of sputtered hafnium oxide films for sensor applications. In: Theil JA, Bohm M, Gardner DS, Blalock T (eds) *Materials, Integration and Technology for Monolithic Instruments*, Warrendale, 2005. Materials Research Society Symposium Proceedings. Materials Research Society, pp 145-150
- Huang XY, Xu Z, Chen LD (2004) The thermoelectric performance of ZrNiSiVZrO<sub>2</sub> composites. *Solid State Commun* 130 (3-4):181-185. doi:10.1016/j.ssc.2004.02.001
- Kappe CO, Stadler A (2005) *Microwaves in Organic and Medicinal Chemistry*. WILEY-VCH Weinheim
- Matsumoto K, Mele P (2010) Artificial pinning center technology to enhance vortex pinning in YBCO coated conductors. *Supercond Sci Technol* 23 (1). doi:014001  
10.1088/0953-2048/23/1/014001

- Meskin PE, Sharikov FY, Ivanov VK, Churagulov BR, Tretyakov YD (2007) Rapid formation of nanocrystalline HfO<sub>2</sub> powders from amorphous hafnium hydroxide under ultrasonically assisted hydrothermal treatment. *Mater Chem Phys* 104 (2-3):439-443. doi:10.1016/j.matchemphys.2007.03.042
- Molina J, Munoz AL, Calleja W, Rosales P, Torres A (2012a) High-quality spin-on glass-based oxide as a matrix for embedding HfO<sub>2</sub> nanoparticles for metal-oxide-semiconductor capacitors. *Journal of Materials Science* 47 (5):2248-2255. doi:10.1007/s10853-011-6036-0
- Molina J, Ortega R, Calleja W, Rosales P, Zuniga C, Torres A (2012b) MOHOS-type memory performance using HfO<sub>2</sub> nanoparticles as charge trapping layer and low temperature annealing. *Mater Sci Eng B-Adv Funct Solid-State Mater* 177 (16):1501-1508. doi:10.1016/j.mseb.2012.02.029
- Niederberger M, Garnweitner G (2006) Organic reaction pathways in the nonaqueous synthesis of metal oxide nanoparticles. *Chem-Eur J* 12 (28):7282-7302. doi:10.1002/chem.200600313
- Niederberger M, Garnweitner G, Krumeich F, Nesper R, Colfen H, Antonietti M (2004a) Tailoring the surface and solubility properties of nanocrystalline titania by a nonaqueous in situ functionalization process. *Chem Mat* 16 (7):1202-1208. doi:10.1021/cm031108r
- Niederberger M, Garnweitner G, Pinna N, Antonietti M (2004b) Nonaqueous and halide-free route to Crystalline BaTiO<sub>3</sub>, SrTiO<sub>3</sub>, and (Ba,Sr)TiO<sub>3</sub> nanoparticles via a mechanism involving C-C bond formation. *J Am Chem Soc* 126 (29):9120-9126. doi:10.1021/ja0494959
- Obradors X, Puig T, Ricart S, Coll M, Gazquez J, Palau A, Granados X (2012) Growth, nanostructure and vortex pinning in superconducting YBa<sub>2</sub>Cu<sub>3</sub>O<sub>7</sub> thin films based on trifluoroacetate solutions. *Supercond Sci Technol* 25 (12). doi:10.1088/0953-2048/25/12/123001
- Olliges-Stadler I, Rossell MD, Niederberger M (2010) Co-operative Formation of Monolithic Tungsten Oxide-Polybenzylene Hybrids via Polymerization of Benzyl Alcohol and Study of the Catalytic Activity of the Tungsten Oxide Nanoparticles. *Small* 6 (8):960-966. doi:10.1002/smll.200902289
- Park J, Joo J, Kwon SG, Jang Y, Hyeon T (2007) Synthesis of monodisperse spherical nanocrystals. *Angew Chem-Int Edit* 46 (25):4630-4660. doi:10.1002/anie.200603148
- Pinna N, Garnweitner G, Antonietti M, Niederberger M (2004) Non-aqueous synthesis of high-purity metal oxide nanopowders using an ether elimination process. *Adv Mater* 16 (23-24):2196. doi:10.1002/adma.200400460
- Pinna N, Grancharov S, Beato P, Bonville P, Antonietti M, Niederberger M (2005) Magnetite nanocrystals: Nonaqueous synthesis, characterization, and solubility. *Chem Mat* 17 (11):3044-3049. doi:10.1021/cm050060+
- Pucci A, Clavel G, Willinger MG, Zitoun D, Pinna N (2009) Transition Metal-Doped ZrO<sub>2</sub> and HfO<sub>2</sub> Nanocrystals. *Journal of Physical Chemistry C* 113 (28):12048-12058. doi:10.1021/jp9029375
- Ramadoss A, Kim SJ (2012) Synthesis and characterization of HfO<sub>2</sub> nanoparticles by sonochemical approach. *J Alloy Compd* 544:115-119. doi:10.1016/j.jallcom.2012.08.005
- Ramadoss A, Krishnamoorthy K, Kim SJ (2012) Novel synthesis of hafnium oxide nanoparticles by precipitation method and its characterization. *Mater Res Bull* 47 (9):2680-2684. doi:10.1016/j.materresbull.2012.05.051

- Rinkio M, Johansson A, Paraoanu GS, Torma P (2009) High-Speed Memory from Carbon Nanotube Field-Effect Transistors with High-kappa Gate Dielectric. *Nano Lett* 9 (2):643-647. doi:10.1021/nl8029916
- Stefanic G, Music S, Molanov K (2005) The crystallization process of HfO<sub>2</sub> and ZrO<sub>2</sub> under hydrothermal conditions. *J Alloy Compd* 387 (1-2):300-307. doi:10.1016/j.jallcom.2004.06.064
- Tang J, Fabbri J, Robinson RD, Zhu YM, Herman IP, Steigerwald ML, Brus LE (2004) Solid-solution nanoparticles: Use of a nonhydrolytic sol-gel synthesis to prepare HfO<sub>2</sub> and Hf<sub>x</sub>Zr<sub>1-x</sub>O<sub>2</sub> nanocrystals. *Chem Mat* 16 (7):1336-1342. doi:10.1021/cm049945w
- Tirosh E, Markovich G (2007) Control of defects and magnetic properties in colloidal HfO<sub>2</sub> nanorods. *Adv Mater* 19 (18):2608. doi:10.1002/adma.200602222
- Tobita H, Notoh K, Higashikawa K, Inoue M, Kiss T, Kato T, Hirayama T, Yoshizumi M, Izumi T, Shiohara Y (2012) Fabrication of BaHfO<sub>3</sub> doped Gd<sub>1</sub>Ba<sub>2</sub>Cu<sub>3</sub>O<sub>7-delta</sub> coated conductors with the high I-c of 85 A/cm-w under 3 T at liquid nitrogen temperature (77 K). *Supercond Sci Technol* 25 (6):062002. doi:10.1088/0953-2048/25/6/062002
- Trikeriotis M, Krysak M, Chung YS, Ouyang C, Cardineau B, Brainard R, Ober CK, Giannelis EP, Cho K (2012) Nanoparticle Photoresists from HfO<sub>2</sub> and ZrO<sub>2</sub> for EUV Patterning. *J Photopolym Sci Technol* 25 (5):583-586
- Van Driessche I, Feys J, Hopkins SC, Lommens P, Granados X, Glowacki BA, Ricart S, Holzappel B, Vilardell M, Kirchner A, Backer M (2012) Chemical solution deposition using ink-jet printing for YBCO coated conductors. *Supercond Sci Technol* 25 (6). doi:10.1088/0953-2048/25/6/065017
- Waldorf AJ, Dobrowolski JA, Sullivan BT, Plante LM (1993) Optical coatings deposited by reactive ion plating. *Appl Optics* 32 (28):5583-5593
- Wilk GD, Wallace RM, Anthony JM (2001) High-kappa gate dielectrics: Current status and materials properties considerations. *J Appl Phys* 89 (10):5243-5275. doi:10.1063/1.1361065